Mechanics Research Communications 52 (2013) 25–31

Contents lists available at SciVerse ScienceDirect

Mechanics Research Communications

journal homepage: www.elsevier.com/locate/mechrescom

Voltage–amplitude response of alternating current near half natural frequency electrostatically actuated MEMS resonators

Dumitru I. Caruntu*, Israel Martinez, Kyle N. Taylor

University of Texas-Pan American, Mechanical Engineering Department, Edinburg, TX 78541, USA

ARTICLE INFO

Article history:
Received 7 November 2012
Received in revised form 10 April 2013
Accepted 7 June 2013
Available online xxx

Keywords:
MEMS resonators
Nonlinear dynamics
Soft AC excitation
Primary resonance
Voltage response

ABSTRACT

This paper uses the Reduced Order Model (ROM) method to investigate the nonlinear-parametric dynamics of electrostatically actuated MEMS cantilever resonators under soft Alternating Current (AC) voltage of frequency near half natural frequency of the resonator. The voltage is between the resonator and a ground plate, and provides a nonlinear parametric actuation for the resonator. Fringe effect and damping forces are included. The resonator is modeled as an Euler–Bernoulli cantilever. Two methods of investigations are compared, Method of Multiple Scales (MMS), and Reduced Order Model. Moreover, the instabilities (bifurcation points) are predicted for both cases, when the voltage is swept up, and when the voltage is swept down. Although MMS and ROM are in good agreement for small amplitudes, MMS fails to accurately predict the behavior of the MEMS resonator for greater amplitudes. Only ROM captures the behavior of the system for large amplitudes. ROM convergence shows that five terms model accurately predicts the steady-states of the resonator for both small and large amplitudes.

1. Introduction

Due to their attractive features, Microelectromechanical Systems (MEMS) devices have gained tremendous interest over the years. Excellent review papers have been reported in the literature, Bogue (2007), Chuang et al. (2010), Tanaka (2007), and van Beek and Puers (2012). Microbeams are used extensively in applications such as switches, filters, resonators, accelerometers and sensors, Dumas et al. (2011), Badri et al. (2010), Tang et al. (2011), Dai et al. (2011), and Zhang et al. (2011). Accelerometers are used in many fields, from automobile (air-bag sensor and rollover detection sensor) to mobile phone applications, Braghin et al. (2007). Besides piezoelectric and electro-magnetic actuation methods, electrostatic actuation is also used in driving and sensing such systems, Stulemeijer et al. (2009) and Abdel-Rahman et al. (2003). Electrostatic actuation offers the advantage of providing enough force that can be controlled through an electric supply requiring low energy consumption. Since these resonators are small in size, they have to be driven close to or even into nonlinear regimes to store enough energy for sufficiently good signal to noise ratio, Mestrom et al. (2008). Nonlinearity usually arises from sources such as the electrostatic actuation itself, squeeze-film damping, geometric nonlinearities and intermolecular forces, i.e. Casimir and van der Waals. Intermolecular forces become predominant with continuous reduction in device size, usually occurring at the submicron scales, Ramezani et al. (2007). Clamped–clamped micro-switches under electrical actuation have been investigated, Jia et al. (2012). A perturbation-based method has been used to obtain the amplitude–frequency response, which then has been then compared with experimental data. Yet, voltage response has not been investigated. The dynamic pull-in phenomenon for a clamped–clamped microbeam using Reduced Order Model (ROM) method has also been reported in the literature, Nayfeh et al. (2007). Moreover, the amplitude–voltage response of MEMS resonators under super-harmonic excitation, Younis et al. (2004), has been obtained using a perturbation-based method and validated using ROM. Al Saleem and Younis (2009) investigated the dynamic pull-in escape in electrostatic MEMS. Amplitude–frequency responses have been generated using simulation and experimental results. Yet, the system was modeled as a nonlinear single-degree-of-freedom model (lumped system). However, the amplitude–voltage response of MEMS cantilever resonators for AC actuation frequency near the system's half natural frequency has been reported in the literature, Caruntu and Martinez (2012). Yet, results were numerically obtained using only a two term ROM. A subsequent investigation used both the Method of Multiple Scales (MMS) and a five term ROM, Caruntu et al. (2013). Yet, only amplitude–frequency response has been investigated. To the best of our knowledge, investigations reported in the literature are limited to either (1) the pull-in phenomenon for clamped–clamped microbeams, (2) lumped models, (3) influence of parameters other than air damping and fringe effect, (4) MMS, or (5) ROM.

* Corresponding author. Tel.: +1 956 665 2079; fax: +1 956 665 3527.
E-mail addresses: caruntud@utpa.edu, caruntud2@asme.org, dcaruntu@yahoo.com (D.I. Caruntu).

0093-6413/$ – see front matter © 2013 Elsevier Ltd. All rights reserved.
http://dx.doi.org/10.1016/j.mechrescom.2013.06.001

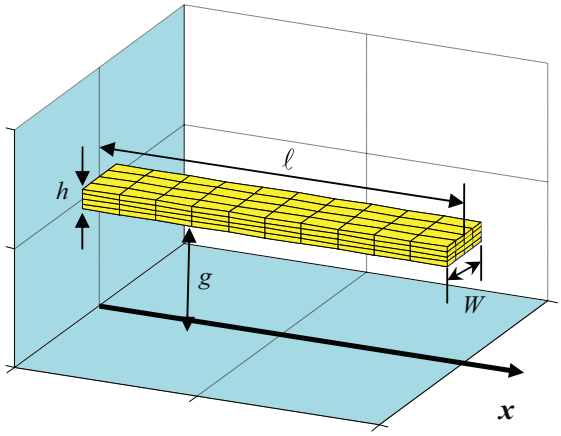

Fig. 1. Uniform MEMS resonator.

This paper deals with the amplitude–voltage response of MEMS resonator cantilevers under soft electrostatic actuation. The electrostatic actuation is of AC voltage of frequency near half natural frequency (resulting in primary resonance) of the system. This is a nonlinear parametric excitation. This is for the first time when for the amplitude–voltage response of such MEMS resonator cantilevers (1) a ROM (based on the Galerkin procedure) up to five terms is employed to develop a set of non-explicit ordinary differential equations and AUTO 07P software is used to numerically obtain the amplitude–voltage response, (2) a direct comparison between MMS and ROM method using two-, three-, four-, and five-term is reported, (3) the influences of AC frequency of actuation, air damping, and fringe correction on the response using both MMS and ROM are provided. This work shows that the instabilities for high amplitudes of the resonator are not captured by the MMS. Only four or five term ROM would capture this behavior.

2. Differential equation of motion

Fig. 1 shows an electrostatically actuated MEMS cantilever resonator that consists of a deformable electrode suspended over a ground plate. The dimensionless boundary value problem is given by Caruntu et al. (2013) and Caruntu and Knecht (2011a) as follows:

$$\begin{cases} A^*(z)\dfrac{\partial^2 u(\tau,z)}{\partial \tau^2}+\dfrac{\partial^2}{\partial z^2}\left(I^*(z)\dfrac{\partial^2 u(\tau,z)}{\partial z^2}\right)=-b^*\dfrac{\partial u(\tau,z)}{\partial \tau}+\dfrac{\delta\cdot V^2(\tau)}{[1-u(\tau,z)]^2}+\dfrac{f\cdot\delta\cdot V^2(\tau)}{[1-u(\tau,z)]} \\ u(\tau,0)=\dfrac{\partial u}{\partial z}(\tau,0)=\dfrac{\partial^2 u}{\partial z^2}(\tau,1)=\dfrac{\partial^3 u}{\partial z^3}(\tau,1)=0 \end{cases} \tag{1}$$

where $u=u(z,t)$, z and τ are dimensionless beam transverse displacement, dimensionless longitudinal coordinate, and dimensionless time, respectively. These dimensionless variables are as follows:

$$u=\frac{w}{g};z=\frac{x}{\ell};\tau=t\cdot\frac{1}{\ell^2}\sqrt{\frac{EI_0}{\rho A_0}} \tag{2}$$

where w is the dimensional transverse displacement of the cantilever, x the dimensional longitudinal coordinate, t dimensional time, ℓ is the beam length, g is the gap, ρ the density, and E Young modulus. Dimensionless cross section area A^* and moment of inertia I^* are

$$A^*=\frac{A}{A_0},I^*=\frac{I}{I_0} \tag{3}$$

where A and I are current cross-section area and moment of inertia. In the case of uniform beams, A^* and I^* are equal to one. A_0, I_0, and ℓ are the reference cross-section area, reference cross-section moment of inertia, and beam length, respectively. If uniform cantilevers, then they are the cross-section area and moment of inertia of the cantilever. If the cantilevers are nonuniform, then they could be considered where the cross-section area is maximum, Caruntu (2007, 2009a).

The first term at the right hand side of Eq. (1) is the dimensionless damping force, the second term is the dimensionless electrostatic force, and the last term is the additional electrostatic force due to fringe effect. The dimensionless voltage $V(\tau)$ considered in this work is given by

$$V(\tau)=\cos\Omega^*\tau \tag{4}$$

The dimensionless parameters in Eq. (1) are b^* the dimensionless damping coefficient, δ the dimensionless amplitude of the electrostatic excitation force (also called dimensionless voltage parameter), f the dimensionless fringe coefficient, and Ω^* the dimensionless frequency of excitation, and they are as follows, Caruntu and Knecht (2011a), and Caruntu et al. (2013):

$$b^*=\frac{b}{g}\sqrt{\frac{\ell^4}{\rho A_0 EI_0}},\quad \delta=\frac{\varepsilon_0 W\ell^4}{2g^3EI_0}V_0^2,$$
$$f=\frac{0.65g}{W},\quad \Omega^*=\Omega\ell^2\sqrt{\frac{\rho A_0}{EI_0}} \tag{5}$$

where V_0 is the amplitude of the AC voltage, b the viscous damping per unit length coefficient, W the beam width and ε_o the permittivity of free space.

3. Soft AC voltage frequency near half natural frequency

The frequency of the AC voltage is near half the natural frequency, $\Omega^*\approx\omega_k/2$ in this work. The nearness of the excitation frequency can be written as

$$2\Omega^*=\omega_k+\sigma \tag{6}$$

where σ is a detuning parameter. Substituting Eqs. (4) and (6) into Eq. (1), it results

$$\frac{\partial^4 u(\tau,z)}{\partial z^4}+\frac{\partial^2 u(\tau,z)}{\partial \tau^2}+b^*\frac{\partial u(\tau,z)}{\partial \tau}=\left\{\frac{\delta}{[1-u(\tau,z)]^2}+\frac{f\cdot\delta}{[1-u(\tau,z)]}\right\}\frac{(1+\cos 2\Omega^*\tau)}{2} \tag{7}$$

One can notice that although the frequency of the AC voltage is near half natural frequency, the frequency of the excitation force is near natural frequency; notice the cosine in Eq. (7). This is nonlinear-parametric primary resonance of the structure.

4. MMS and ROM of uniform MEMS resonators

The Method of Multiple Scales (MMS) has been used by Caruntu and Knecht (2011a) to investigate the frequency response of the resonator. The steady state response of the resonator has been

Table 1
First five natural frequencies and mode shape coefficients for uniform cantilever.

	$k=1$	$k=2$	$k=3$	$k=4$	$k=5$
ω_k	3.51562	22.0336	61.70102	120.91202	199.85929
C_k	−0.734	−1.0185	−0.9992	−1.00003	−1.00000

Table 2
Dimensional system parameters.

Parameter	Symbol	Value
Beam width	W	20 μm
Beam length	ℓ	300 μm
Beam thickness	h	2.0 μm
Initial gap distance	g	8.0 μm
Material density	ρ	2330 kg/m^3
Young's Modulus	E	169 GPa
Quality factor	Q	350
Peak AC voltage (pull-in in Fig. 2)	V_0	8.88 V
Frequency of excitation	Ω	191526 rad/s

found. In this work the voltage response of the resonator is investigated. The function *fsolve* of the software package Matlab is used to numerically solve the steady-state algebraic equations of the system, Caruntu and Knecht (2011a). The Reduced Order Model (ROM) method is also used to find the voltage response of the resonator. A system of non-explicit second order differential equations is obtained using ROM. These equations are integrated two ways, one using AUTO to obtain the voltage–amplitude response (bifurcation diagrams), and the other using Matlab to obtain the time response and confirm the results obtained using AUTO. ROM is based on the Galerkin procedure and uses the undamped linear mode shapes of the cantilever beam as the basis functions, Caruntu et al. (2013), Caruntu and Knecht (2011a), and Caruntu and Solis Silva (2011b). The solution of Eq. (7) is assumed as

$$u(z,\tau)=\sum_{i=1}^{N}u_i(\tau)\phi_i(z) \tag{8}$$

where N is the number of terms, $u_i(\tau)$ time dependent coefficients, and $\phi_i(z)$ the set of first N linear undamped mode shapes of the uniform cantilever beam given by Caruntu and Knecht (2011a)

$$\phi_k(z)=-\left\{\cos\left(\sqrt{\omega_k}z\right)-\cosh\left(\sqrt{\omega_k}z\right)+C_k\left[\sin\left(\sqrt{\omega_k}z\right)-\sinh\left(\sqrt{\omega_k}z\right)\right]\right\} \tag{9}$$

Moreover k is any nonzero positive integer, and ω_k are the corresponding natural frequencies. The first five natural frequencies ω_k and coefficients C_k from Eq. (9) are given in Table 1. The mode shapes given by Eq. (9) are with respect to the dimensionless longitudinal coordinate z of the cantilever, and the natural frequencies given in Table 1 are dimensionless. Since they are not related to specific dimensions, they can be used for any cantilever under investigation, including the cantilever given afterwards in Table 2 for numerical simulations.

In order to implement the ROM method the following steps are considered. Eq. (7) is multiplied by $[1-u(\tau,z)]^2$ (to eliminate any displacement $u(z,\tau)$ from appearing in the denominator, Caruntu and Knecht, 2011a), and then Eq. (8) is substituted into it. Since the following relationships are satisfied by the mode shapes of the cantilever

$$u^{(4)}=\sum_{i}^{N}u_i\phi_i^{(4)}=\sum_{i}^{N}\omega_i^2u_i\phi_i \tag{10}$$

the resulting equation is as follows:

$$\begin{aligned}&\sum_{i}^{N}\ddot{u}_i\phi_i-2\sum_{ij}^{N}\ddot{u}_iu_j\phi_i\phi_j+\sum_{ijk}^{N}\ddot{u}_iu_ju_k\phi_i\phi_j\phi_k+b^*\sum_{i}^{N}\dot{u}_i\phi_i\\&-2b^*\sum_{ij}^{N}\dot{u}_iu_j\phi_i\phi_j+b^*\sum_{ijk}^{N}\dot{u}_iu_ju_k\phi_i\phi_j\phi_k+\sum_{i}^{N}\omega_i^2u_i\phi_i\\&-2\sum_{ij}^{N}\omega_i^2u_iu_j\phi_i\phi_j+\sum_{ijk}^{N}\omega_i^2u_iu_ju_k\phi_i\phi_j\phi_k\\&=\delta V^2(\tau)+f\delta V^2(\tau)-f\delta V^2(\tau)\sum_{i}^{N}u_i\phi_i\end{aligned} \tag{11}$$

Then Eq. (11) is multiplied by mode shape $\phi_n(z)$ and the entire equation is integrated from $z=0$ to 1, where $n=1, 2, \ldots N$. The orthonormality of the mode shapes $\phi_i(z)$ is given by

$$\int_0^1\phi_i\phi_j dz=\delta_{ij}=\begin{cases}0 & ,i\neq j\\1 & ,i=j\end{cases} \tag{12}$$

Therefore, depending on the number of terms used, this process leads to a system of second order coupled differential equations in time as follows:

$$\begin{aligned}&\ddot{u}_n-2\sum_{ij}^{N}\ddot{u}_iu_j\int_0^1\phi_i\phi_j\phi_n dz+\sum_{ijk}^{N}\ddot{u}_iu_ju_k\int_0^1\phi_i\phi_j\phi_k\phi_n dz+b^*\dot{u}_n\\&-2b^*\sum_{ij}^{N}\dot{u}_iu_j\int_0^1\phi_i\phi_j\phi_n dz+b^*\sum_{ijk}^{N}\dot{u}_iu_ju_k\int_0^1\phi_i\phi_j\phi_k\phi_n dz+\omega_n^2u_n\\&-2\sum_{ij}^{N}\omega_i^2u_iu_j\int_0^1\phi_i\phi_j\phi_n dz+\sum_{ijk}^{N}\omega_i^2u_iu_ju_k\int_0^1\phi_i\phi_j\phi_k\phi_n dz\\&=(1+f)\delta V^2(\tau)\int_0^1\phi_n dz-f\delta V^2(\tau)u_n\end{aligned} \tag{13}$$

where $n=1, 2, \ldots, N$. The system of N second order differential Eq. (13) is then transformed into a system of $2N$ first order differential equations. The system of differential equations is then integrated for four cases $N=2$, $N=3$, $N=4$, and $N=5$ using AUTO 07P, a software package for continuation and bifurcation problems providing the steady-state solutions, both stable and unstable. In AUTO the computation of periodic solutions to a periodically forced system can be done by adding a nonlinear oscillator with the desired periodic forcing as one of the solution components, Doedel and Oldeman (2009). The voltage–amplitude response of the system under AC voltage near half natural frequency is investigated using a ROM from two to five term ROM. Pull-in instability is predicted. Also, the system of $2N$ first order differential equations is directly integrated using the software package Matlab to numerically simulate the time response for various cases, and consequently confirm the ROM results obtained using AUTO.

Table 3
Dimensionless system parameters.

Damping coefficient	b^*	0.01
Frequency parameter	σ	−0.01
Fringe coefficient	f	0.26
Amplitude of excitation (pull-in in Fig. 2)	δ	0.049

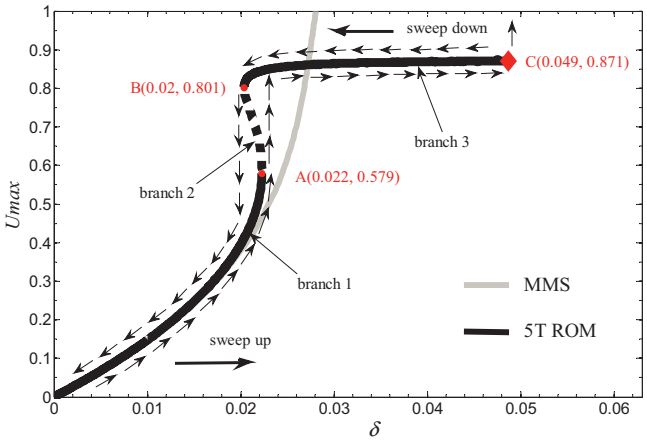

Fig. 2. Amplitude–voltage response near half natural frequency using the MMS and five term ROM for dimensionless parameter values $b^* = 0.01$, $\sigma = -0.01$ and $f = 0.26$.

5. Numerical simulations

Tables 2 and 3 give the dimensional and dimensionless parameters, respectively, for which numerical simulations are conducted. Fig. 2 also called bifurcation diagram shows the amplitude–voltage response for five terms (5 T) ROM, where U_{max} is the amplitude of the tip (free end) of the resonator, and δ is the dimensionless voltage parameter. This response consists of three branches. Branches 1 and 3 show stable steady-state solutions (solid lines), and branch 2 unstable solutions (dash lines), Caruntu and Knecht (2011a, 2009b). As the voltage is swept up, the amplitude of the resonator increases, along branch 1, until reaches point *A* where a sudden jump to branch 3 of high amplitudes occurs. As the voltage continues to be swept up the amplitude slightly increases along branch 3 until it reaches point *C* where a sudden jump to pull-in occurs.

The voltage of point *C* is called hereafter pull-in voltage. In Fig. 2, the pull-in voltage is $\delta_c = 0.049$ and corresponds to $V_o = 8.88$ *V*, Table 2. Conversely, if the amplitude of the resonator is on branch 3 and the voltage is swept down, then the amplitude of the resonator decreases along branch 3 until reaches point *B* where a sudden jump to branch 1 of lower amplitudes occurs. Branches 1 and 2 together and branches 2 and 3 together are two saddle-node bifurcations with *A* and *B* bifurcation points, respectively, called hereafter saddle-node bifurcation point *A* and saddle-node bifurcation point *B*. Fig. 2 also shows the amplitude–voltage response using MMS with Taylor expansions up to the third power of the electrostatic force to include fringe effect. One can notice the excellent agreement between the MMS and ROM for amplitudes less than 0.4 of the gap.

Yet, MMS fails to predict the behavior of the resonator for large amplitudes. MMS underestimates the nonlinear behavior of the system, it fails to predict or overestimates the bifurcation points *A* and *B*, and pull-in instability point *C*, showing just a continuous increase in amplitude with the increase in voltage within the interval (0,1) of U_{max} the amplitude of the free end. The voltage band between the voltage of point *B* and point *C* is called hereafter the large amplitude voltage band.

Time responses in Figs. 3 and 4 are obtained using five terms ROM Matlab simulations. The time responses confirm the results in the bifurcation diagram Fig. 2. Fig. 3 shows the time response of the resonator's tip for two voltage values $\delta = 0.02$ in Fig. 3(a), and $\delta = 0.023$ in Fig. 3(b), for the same damping, frequency, and fringe parameters as in Fig. 2. One can notice in Fig. 3(a) that the resonator has an initial zero amplitude. The amplitude increases and then decreases until settles to a steady-state amplitude of 0.4. One can see that this is in agreement with Fig. 2 which shows an amplitude of 0.4 if $\delta = 0.02$. Similarly, Figs. 3(b) and 2 are in agreement, both showing a steady-state amplitude of 0.8 if $\delta = 0.023$.

Fig. 4 confirms the time response and the pull-in phenomenon that occurs for $\delta = 0.05$ in Fig. 2. Pull-in manifests itself as a sudden increase in resonator tip velocity toward the underlying substrate as the tip reaches its maximum displacement. This leads to contact between the resonator and ground plate. When this occurs, the numerical solution changes so rapidly that the code used to model the system is unable to continue. Fig. 4 illustrates the pull-in phenomenon showing how the resonator loses stability. In the very last part of the motion, the dimensionless velocity *Vmax* of the resonator tip, Fig. 4(c) and detail (d), suddenly increases while the dimensionless deflection *Umax*, Fig. 4(a) and detail (b) of the resonator tip increases to approach unity. There is an inflection point in the upper part of the displacement detail, Fig. 4(b), the concavity changes from concave down to concave up as the cantilever tip begins to move very fast toward pull-in. This type change in deflection concavity before pull-in has been reported by Caruntu and Knecht (2011a).

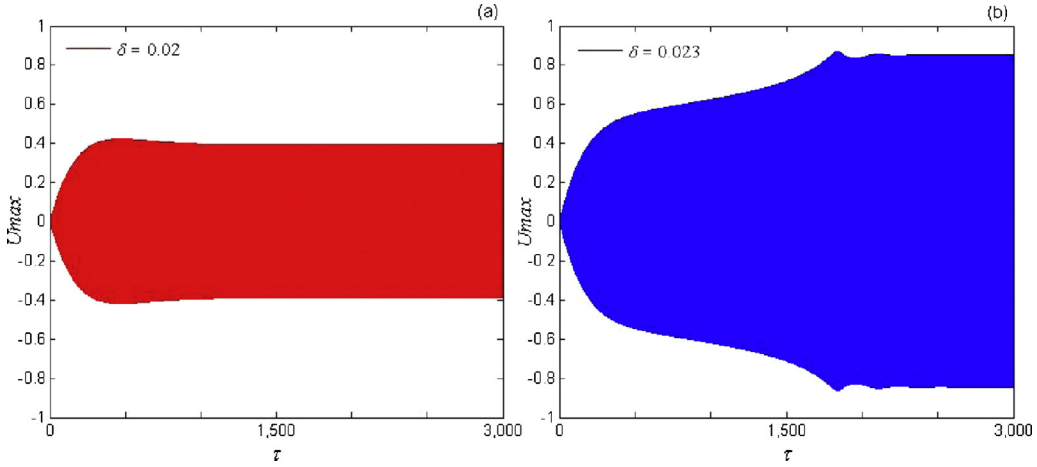

Fig. 3. Time response of the resonator's tip using five term ROM for (a) $\delta = 0.02$ and (b) $\delta = 0.023$. In both cases $b^* = 0.01$; $\sigma = -0.01$; $f = 0.26$.

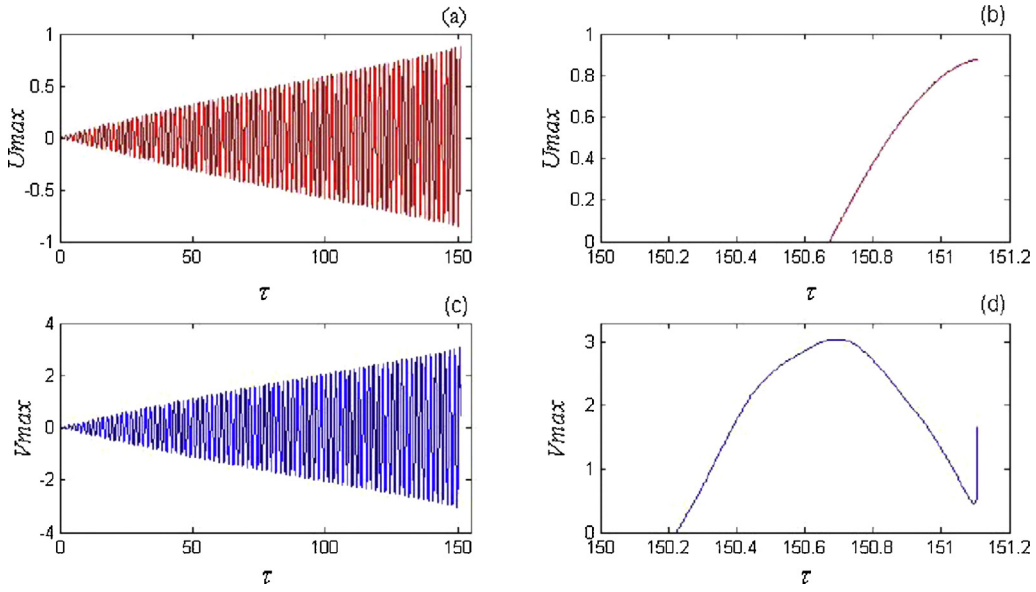

Fig. 4. Time response of the resonator's tip using five term ROM and showing the occurrence of pull-in phenomenon. Parameter values are $b^*=0.01$, $\delta=0.05$, $f=0.26$ and $\sigma=-0.01$. (a) Tip's displacement, (b) displacement detail before pull-in, (c) tip's velocity, and (d) velocity detail before pull-in.

Fig. 5 illustrates the convergence of the ROM method for the voltage–amplitude response with respect to the number of terms $N=2,3,4,5$ used in the ROM, showing that five-term ROM gives excellent predictions of the nonlinear behavior of the MEMS cantilever for large amplitudes and pull-in phenomenon.

Numerical simulations conducted in this research show that four or more terms are required for the ROM to predict pull-in. As the number of terms in the ROM increases from two to five in Fig. 5, the nonlinear behavior of the system is better captured, the bifurcation points are shifted to lower amplitudes and frequencies until they become points *A* and *B* in Fig. 2. Also, with the increase of the number of ROM terms the pull-in voltage and amplitude are shifted to lower values until they become the voltage and amplitude of point *C* in Fig. 2. In other words, two-term ROM and three-term ROM in Fig. 5 do not predict the pull-in phenomenon corresponding to point *C* in Fig. 2, and overestimate the amplitude and voltage of the saddle-node bifurcation points *A* and *B* in Fig. 2.

Fig. 6 shows the effect of the dimensionless damping parameter b^* on the voltage–amplitude response of the resonator using a five term ROM and MMS. For larger damping values $b^*=0.05$ both methods ROM and MMS are in agreement showing a linear behavior of the system for soft AC excitation. As the damping decreases to $b^*=0.01$, ROM predicts (while MMS fails to predict) the two saddle-node bifurcation points, *A* and *B* in Fig. 2, and pull-in corresponding to point *C* in Fig. 2. Additional decrease of damping $b^*=0.005$ results in a shifting to lower voltage of both saddle-node bifurcation points and pull-in voltage, Fig. 6. Less damping translates into lesser amount of energy loss within the MEMS system, meaning the system experiences for soft AC excitations larger amplitudes at a given voltage and jump phenomena. MMS fails to predict the nonlinear behavior of the resonator for amplitudes larger than 0.4 of the gap.

Fig. 7(a) shows the time response for three values of damping, when the voltage parameter is $\delta=0.014$. The steady state amplitudes in Fig. 7(a) are in agreement with those in Fig. 6.

Fig. 8 illustrates the influence of the frequency parameter σ on the voltage–amplitude response of the MEMS resonator using five term ROM and MMS. As σ decreases the nonlinearities in the system are enhanced, the saddle-node bifurcation points and pull-in voltage are born. Additional decrease in frequency of excitation lowers the pull-in voltage (see the right-hand side end point of branch 3), and shifts the bifurcation point *B* to lower voltage values, and the bifurcation point *A* to larger voltage values.

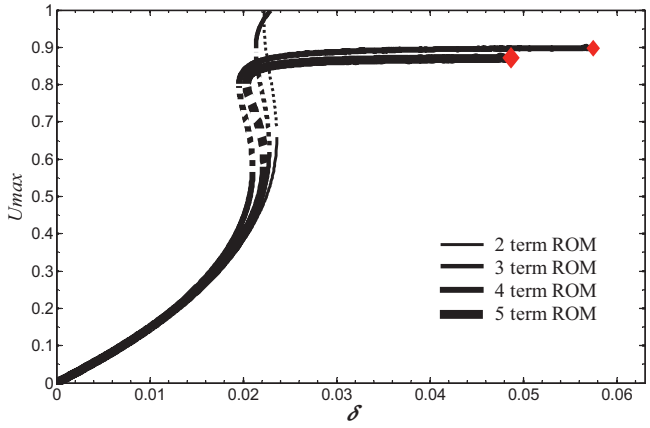

Fig. 5. Amplitude–voltage response near half natural frequency using a two, three, four and five term ROM for dimensionless parameter values $b^*=0.01$, $\sigma=-0.01$ and $f=0.26$.

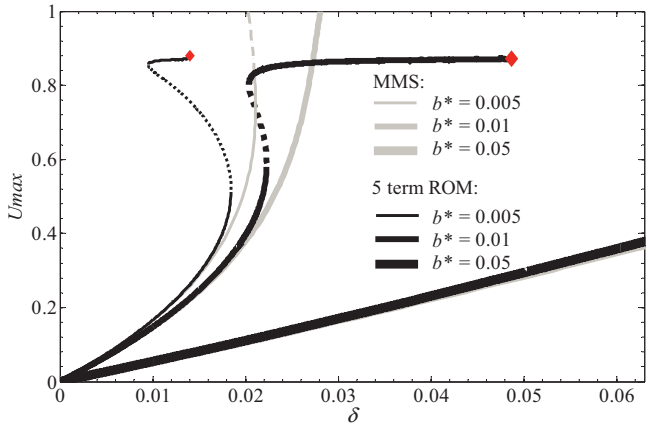

Fig. 6. Amplitude–voltage response showing the influence of the dimensionless damping parameter b^* for dimensionless parameter values $\sigma=-0.01$ and $f=0.26$ using the MMS and a five term ROM.

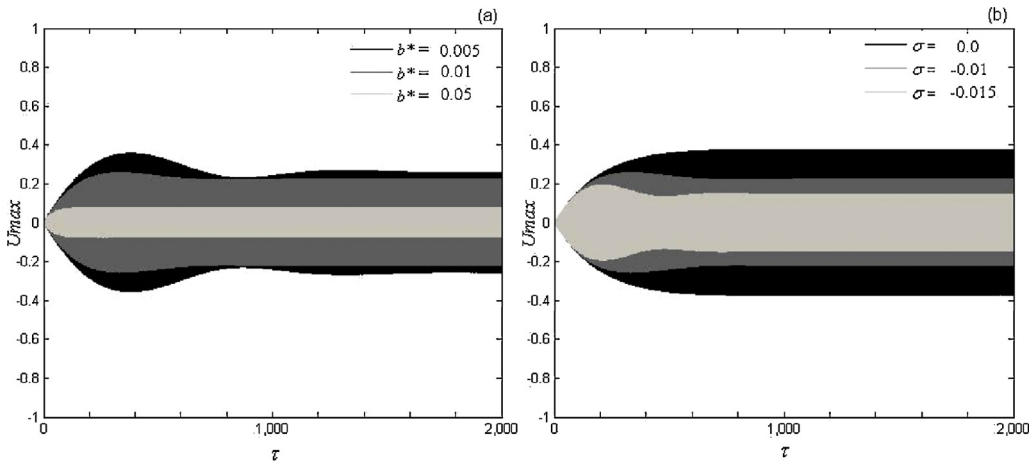

Fig. 7. Time response of the resonator's tip using five term ROM. (a) Influence of damping parameter b^* for $\delta = 0.014$, $\sigma = -0.01$, and $f = 0.26$ and (b) influence of frequency parameter σ for $\delta = 0.014$, $b^* = 0.01$, and $f = 0.26$.

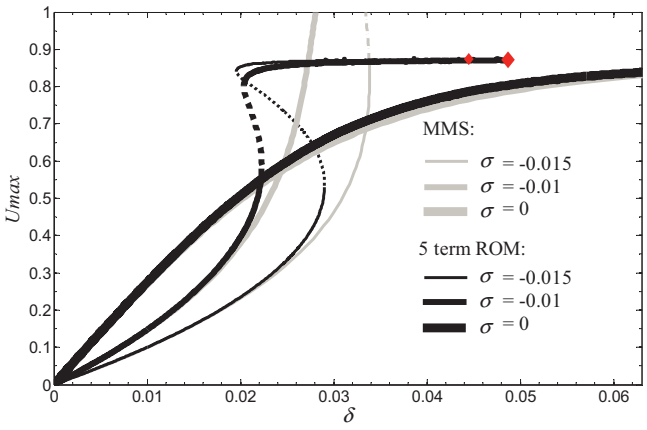

Fig. 8. Amplitude–voltage response showing the influence of frequency σ for dimensionless parameter values $b^* = 0.01$ and $f = 0.26$ using the MMS and a five term ROM.

Fig. 7(b) shows the time response for three values of the frequency parameter, when the voltage parameter is $\delta = 0.014$. The steady state amplitudes in Fig. 7(b) are in agreement with those in Fig. 8.

Fig. 9 shows the influence of the fringe effect correction f on the amplitude–voltage response of the system using five term ROM and MMS. Fringing fields emanating from the lateral and top surfaces of the deformable beam need to be accounted for when modeling the electrostatic field. ROM predicts that as the fringe parameter f increases, the bifurcation points A and B shift to lower voltage as well as the pull-in voltage (point C).

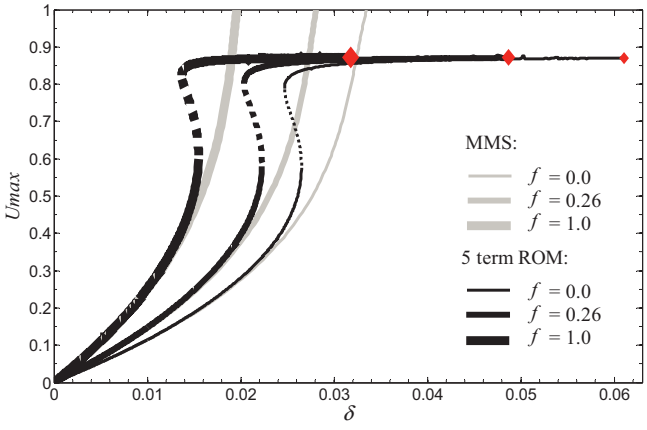

Fig. 9. Amplitude–voltage response showing the influence of the fringe correction f for dimensionless parameter values $b^* = 0.01$ and $\sigma = -0.01$ using the MMS and a five term ROM.

6. Discussion and conclusions

This paper investigated the nonlinear dynamics of MEMS cantilever resonator under soft AC voltage of frequency near resonator's half natural frequency. The resonator is modeled as an Euler–Bernoulli beam. Therefore no nonlinearities arise from the structure itself.

The electrostatic force, including first-order fringe correction, actuating the resonator induces parametric nonlinear resonances. Parametric coefficients are found in both linear and nonlinear terms within the governing equation. ROM method based on the Galerkin procedure has been employed. Two term, three term, four term and five term ROM have been considered in order to show the convergence of the method.

AUTO 07P software has been used to numerically solve the resulting system ODE's and generate the amplitude–voltage response. The predictions of the ROM (present work) and MMS have been discussed. ROM was able to accurately capture the behavior of the system where the perturbation method MMS could not, Younis et al. (2003), i.e. from moderately large deflections up to the pull-in instability limit. Using four or more modes guarantees the prediction of the pull-in phenomenon. This is good agreement with Younis et al. (2003), Nayfeh et al. (2007), and Caruntu and Knecht (2011a). The amplitude–voltage response, ROM convergence, influence of dimensionless damping, influence of dimensionless voltage parameter, and influence of the dimensionless fringe parameter on the amplitude–voltage response are reported.

It is found that the MEMS resonator loses stability in two steps as the voltage is swept up. First it loses stability for amplitudes about 0.55 of the gap jumping to amplitudes of about 0.85 of the gap. Second, as the voltage increases the resonator loses stability and undergoes a pull-in phenomenon at what is called critical voltage. Voltage larger than the critical voltage results in pull-in. If the resonator undergoes large amplitudes of about 0.85 of the gap for a voltage less than critical voltage, then sweeping down the voltage results in a jump to lower amplitudes of about 0.4 of the gap. It is found that decreasing the damping enhances the nonlinear behavior of the resonator. If the damping is small enough, sweeping up the voltage results into a pull-in phenomenon and not a jump to larger amplitudes. Decreasing the frequency also results in a

nonlinear behavior of the resonator. As the frequency decreases the difference between sweeping up and sweeping down bifurcation voltages (where instability occurs) increases, and the range of voltages for which large amplitudes of about 0.85 of the gap occur reduces. Increasing the fringe effect (increasing the gap to width ratio) results in a shift of the bifurcation voltages (instability voltages) to lower values, and a reduction of the voltage range for which stable large amplitudes exist.

A first limitation of this paper is the use of only Palmer's formula for fringe effect. Other formulas such as Meijs–Fokkema (Caruntu and Knecht, 2011a), and Batra–Porfiri–Spinello (Batra et al., 2006), which are developed for narrow structures, would have had allowed for numerical simulations of narrower structures than the one presented in this work. However, the geometry of the MEMS resonator in this paper does not necessarily require either Meijs–Fokkema or Batra–Porfiri–Spinello fringe formulas. Batra–Porfiri–Spinello formula was derived for narrow microbeams with a ratio width/height between 0.5 and 2.0, while in this work this ratio is 10. Also, Batra et al. (2006) reported that Palmer formula gives erroneous values of the capacitance per unit line for narrow microbeams when the ratio width/thickness is between 0.5 and 5, and the ratio gap/thickness is between 0.2 and 2. The corresponding ratios in this work are 10 and 4. A second limitation of this work is that experimental results are not reported, and a third limitation is that the results reported in this paper are valid only for long (slender) cantilevers for which Euler–Bernoulli theory holds.

Future research will include (1) experimental investigation, (2) influences on system' behavior of other nonlinearities such as squeeze film damping and geometrical nonlinearities, and (3) systems' behavior for higher natural frequencies, i.e. investigations for AC near higher natural frequencies.

Acknowledgements

This material is based on research sponsored by Air Force Research Laboratory under agreement number FA8650-07-2-5061. The U.S. Government is authorized to reproduce and distribute reprints for Governmental purposes notwithstanding any copyright notation thereon. The views and conclusions contained herein are those of the authors and should not be interpreted as necessarily representing the official policies or endorsements, either expressed or implied, of Air Force Research Laboratory or the U.S. Government.

References

Abdel-Rahman, E.M., Nayfeh, A.H., Younis, M.I., 2003. Dynamics of an electrically actuated resonant microsensor. In: Proceedings of the International Conference on MEMS, NANO and Smart Systems (ICMENS'03), IEEE.

Al Saleem, F., Younis, M., 2009. Controlling dynamic pull-in escape in electrostatic MEMS. In: Proceeding of the 6th International Symposium on Mechatronics and its Applications (ISMA 09).

Badri, A.E., Sinha, J.K., Albarbar, A., 2010. A typical filter design to improve the measured signals from MEMS accelerometer. Measurement 43, 1425–1430.

Batra, R.C., Porfiri, M., Spinello, D., 2006. Electromechanical model of electrically actuated narrow beams. Journal of Microelectromechanical Systems 15, 1175–1189.

Bogue, R., 2007. MEMS sensors: past, present, future. Sensor Review 27 (1), 7–13.

Braghin, F., Resta, F., Leo, E., Spinola, G., 2007. Nonlinear dynamics of vibrating MEMS. Sensors and Actuators A 134, 98–108.

Caruntu, D.I., Martinez, I., 2012. VCB2012-78 ROM for amplitude–voltage response of MEMS cantilever resonators under AC actuation of frequency near half-natural frequency. In: Proceedings of the 18th Symposium on Vibrations, Chocs et Bruit, Centre de recherché EDF de Clamart, FR (The French Mechanical Society, July 3–5, 2012.

Caruntu, D.I., Martinez, I., Knecht, M.W., 2013. Reduced order model analysis of frequency response of AC near half natural frequency electrostatically actuated MEMS cantilever. Journal of Computational Nonlinear Dynamics 8, 031011–31021.

Caruntu, D.I., Knecht, M.W., 2011a. On nonlinear response near half natural frequency of electrostatically actuated microresonators. International Journal of Structural Stability and Dynamics 11 (4), 641–672.

Caruntu, D.I., Solis Silva, J.C., 2011b. IMECE2011-64854 Reduced order model of MEMS sensors near natural frequency. In: ASME Proceedings of International Mechanical Engineering Congress and Exposition 2011.

Caruntu, D.I., 2009a. Dynamic modal characteristics of transverse vibrations of cantilevers of parabolic thickness. Mechanics Research Communications 33 (3), 391–404.

Caruntu, D.I., Knecht, M., 2009b. IMECE2009-10663 Parametric response of capacitive sensors near half of natural frequency. In: ASME Proceedings of International Mechanical Engineering Congress and Exposition 2009.

Caruntu, D.I., 2007. Classical Jacobi polynomials, closed-form solutions for transverse vibrations. Journal of Sound and Vibration 306 (3–5), 467–494.

Chuang, W.-C, Lee, H.-L., Chang, P.-Z., Hu, Y.-C., 2010. Review on the modeling of electrostatic MEMS. Sensors 10, 6149–6171.

Dai, G., Li, M., He, X., Du, L., Shao, B., Su, W., 2011. Thermal drift analysis using a multiphysics model of bulk silicon MEMS capacitive accelerometer. Sensors and Actuators A 172, 369–378.

Doedel, E.J., Oldeman, B.E., 2009. AUTO-07P: Continuation and Bifurcation Software for Ordinary Differential Equations. Concordia University, Montréal, Canada.

Dumas, N., Trigona, C., Pons, P., Latorre, L., Nouet, P., 2011. Design of smart drivers for electrostatic MEMS switches. Sensors and Actuators A: Physical 167, 422–432.

Jia, X.L., Yang, J., Kitipornchai, S., Lim, C.W., 2012. Resonance frequency response of geometrically nonlinear micro-switches under electrical actuation. Journal of Sound and Vibration 331, 3397–3411.

Mestrom, R.M.C., Fey, R.H.B., van Beek, J.T.M., Phan, K.L., Nijmeijer, H., 2008. Modelling the dynamics of a MEMS resonator: simulations and experiments. Sensors and Actuators A 142, 306–315.

Nayfeh, A.H., Younis, M.I., Abdel-Rahman, E.M., 2007. Dynamic pull-in phenomenon in MEMS resonators. Nonlinear Dynamics 48, 153–163.

Ramezani, A., Alasty, A., Akbari, J., 2007. Closed-form solutions of the pull-in instability in nano-cantilevers under electrostatic and intermolecular surface forces. International Journal of Solids and Structures 44, 4925–4941.

Stulemeijer, J., Bielen, J.A., Steeneken, P.G., Bouwe van der Berg, J., 2009. Numerical path following as an analysis method for electrostatic MEMS. Journal of Microelectromechanical Systems 18 (2), 488–499.

Tanaka, M., 2007. An industrial and applied review of new MEMS devices features. Microelectronic Engineering 84 (2007), 1341–1344.

Tang, M., Cagliani, A., Davis, Z.J., 2011. Pulse mode readout of MEMS bulk disk resonator based mass sensor. Sensors and Actuators A: Physical 168, 39–45.

van Beek, J.T.M, Puers, R., 2012. A review of MEMS oscillators for frequency reference and timing applications. J. Micromech. Microeng. 22, 013001, http://dx.doi.org/10.1088/0960-1317/22/1/013001.

Younis, M.I., Abdel-Rahman, E.M., Nayfeh, A.H., 2004. Global dynamics of MEMS resonators under superharmonic excitation. In: Proceedings of the 2004 International Conference on MEMS, NANO and Smart Systems, (ICMENS'04), IEEE.

Younis, M.I., Abdel-Rahman, E.M., Nayfeh, A.H., 2003. A reduced-order model for electrically actuated microbeam-based MEMS. Journal of Microelectromechanical Systems 12 (5), 672–680.

Zhang, Z., Liao, X., Han, L., Cheng, Y., 2011. A GaAs MMIC-based coupling RF MEMS power sensor with both detection and non-detection states. Sensors and Actuators A 168, 30–38.